ACI MATERIALS JOURNAL TECHNICAL PAPER

Title no. 102-M51

Uniaxial Stress-Strain Relationship of Spirally Confined Concrete

by Hau Yan Leung and Chris J. Burgoyne

A theoretical model is developed to describe the uniaxial stress-strain relationship of spirally confined concrete. As well as using one single spiral, concrete confined by two interlocking spirals is also studied, using a finite element model to determine the magnification factors caused by multiple confinement. Predictions for the behavior of compression specimens with various types of reinforcement are given. Methods of determining the behavior of concrete in the compression zone of beams in flexure, which are subjected to strains that vary through the depth, are also presented. Experimental verification is not presented herein but has been carried out and is referred to in other work.

Keywords: analytical model; aramid; axial stress; compression; fibers; spirals.

INTRODUCTION

The advent of fiber-reinforced polymer (FRP) as reinforcement or as prestressing tendons for concrete has many advantages because it is more durable than steel. However, it shows no ductility before failure (although its large strain capacity normally means it is are unlikely to snap), which means that beams will normally be designed to be over-reinforced. Thus, instead of failure being initiated by yielding of the steel, with the concrete failing later, it will be caused by crushing of the concrete. Up until now, it has been enough to say that the concrete has sufficient strength, without requiring an extensive understanding of the actual failure process; however, if the concrete is going to fail first, more detail is required.

It is also desirable for the concrete to have greater ductility and, to this end, it has been suggested[1] that spirals of reinforcement should be included in the compression zone (with their axes aligned parallel to the compressive force) to provide additional confinement; if FRPs are being used as the tension reinforcement, it is logical to use them also for the hoop reinforcement. Although rectangular links can be made from steel, they are not ideal for FRP because of strength loss in the corners. In addition, they are less efficient at generating confining stress than circular links.

The applications envisioned are in beams, where it makes both structural and practical sense for them to have rectangular compression flanges. Thus, to maximize the area that is to be confined, it is possible to envision a rectangular compression flange that contains a series of overlapping spirals. There will thus be three types of concrete to be considered—the unconfined concrete in the cover region, the singly confined concrete inside one spiral, and doubly confined concrete in the regions where two spirals overlap (Fig. 1). This paper provides an analytical model for both types of confined concrete; space does not permit the inclusion herein of the tests that have demonstrated the validity of this approach, but they have been carried out and are reported elsewhere.[2] Papers in preparation will report the extension of this work

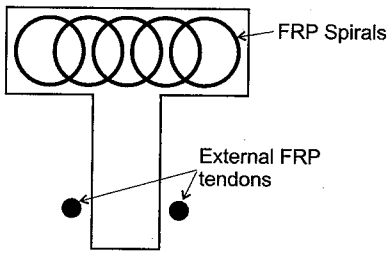

Fig. 1—Novel beam design.

to the determination of the moment-curvature relationship for beams and tests on a full-scale beam with confined compression zone and external aramid prestressing tendons.

Many tests[3-9] have shown that unconfined plain concrete, in particular high-strength concrete, exhibits a brittle failure mode; the failure may be explosive and marks the termination of the stress-strain curve and loss of load-carrying capacity shortly after the peak load. Under deformation control, the stress-strain curve normally includes a monotonically increasing branch up to a peak value, followed by a descending part that gradually flattens to a constant value. The initial portion of the ascending branch is linearly elastic, but at about 70% of the ultimate strength, the presence of microcracks leads to nonlinear behavior, with a reduction in tangent modulus. In the subsequent descending branch, the concrete is severely damaged with prominent cracks. There is a small lateral expansion during the ascending phase, associated with normal Poisson's ratio effects and an increase in volume caused by the microcracks, but the lateral expansion increases dramatically after the peak as the cracks expand.

If there exists a lateral pressure that resists this sideway expansion, however, the core concrete will be in a state of multi-axial compression. It is accepted that when the concrete is experiencing multi-axial compression, both the deformation capacity and strength are improved.[10-17] There are two means of confinement to provide the lateral pressure: active and passive. Both aim to restrict the core concrete from expansion, but the mechanism used to induce the confining pressure is different.

In active confinement, the lateral pressure is applied by an external force whose value is known or can even be controlled in response to the applied load. Kotsovos has presented the results of a study of concrete loaded in this

ACI Materials Journal, V. 102, No. 6, November-December 2005.
MS No. 04-328 received April 15, 2004, and reviewed under Institute publication policies. Pertinent discussion including authors' closure, if any, will be published in the September-October 2006 *ACI Materials Journal* if the discussion is received by June 1, 2006.

Hau Yan Leung *is a lecturer at Chu Hai College, Hong Kong. He received his PhD from the University of Cambridge. His research interests include the behavior of confined concrete in compression.*

ACI member **Chris J. Burgoyne** *is a reader in concrete structures at the Department of Engineering, University of Cambridge. He is a consulting member of ACI Committee 440, Fiber Reinforced Polymer Reinforcement. His research interests include concrete structures reinforced or prestressed with fiber-reinforced polymer.*

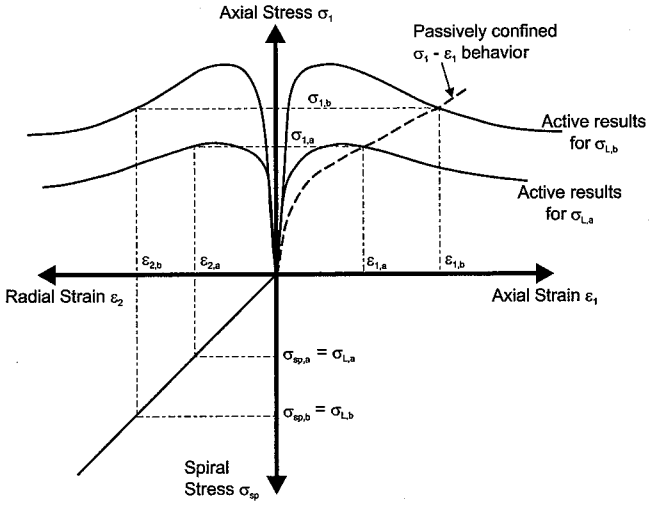

Fig. 2—Schematic model for passive fiber-reinforced polymer confinement.

way, which can be used to determine the relevant load-extension curves. It does not, however, represent the behavior of concrete where the confining stress comes from reinforcement inside, or on the surface of, the concrete.

Passive confinement arises when the lateral expansion of the concrete is resisted by confining reinforcement; the confining pressure is highly dependant on the relationship between axially applied stress and the induced lateral strain. The concrete bears the axial load because of the stress state induced by the lateral reinforcement. In the ascending part of the stress-strain curve, the confining effect is small because the lateral expansion is insignificant, at least until high stress levels, but the descending portion of the stress-strain response is dominated by the behavior of the confining reinforcement that resists the lateral expansion, establishing a multi-axial state of stress in the core concrete.

RESEARCH SIGNIFICANCE

The paper presents an analytical method of determining the stress-strain curve of concrete that is confined by spiral reinforcement that can be either linearly elastic (aramid) or elasto-plastic (steel). Because stress-strain curves can be determined for concrete that is unconfined, confined by a single spiral, or confined by overlapping spirals, and can also be applied to concrete that is not loaded axially, a wide range of cases can be studied. Because the equations presented herein are based on an extensive set of triaxial tests, and are verified in a set of tests reported elsewhere, they can be applied in many different circumstances.

ACTIVELY CONFINED CONCRETE

The analysis presented herein is based on Kotsovos' study of concrete subjected to active hydraulic pressure.[6] It was recognized that most concrete structural members are subjected to a multi-axial stress state. Kotsovos and Newman made a mathematical prediction of the stress-strain response of concrete in terms of the hydrostatic stress σ_o and deviatoric stress τ_o invariants.[18,19] They performed an extensive experimental study to obtain the stress-strain profile of concrete cylinders subjected to different hydraulic pressures and proposed empirical equations. Crack extension was identified as the main cause of fracture; deviatoric stress tends to give a unidirectional fracture in the direction of maximum compressive stress, while hydrostatic stress gives random crack propagation that reduces the rate of fracture caused by the deviatoric stress. Because any state of stress can be decomposed into hydrostatic and deviatoric stresses, the behavior of concrete under a generalized stress condition can be defined by using these components. The work was later extended[6] by introducing the concept of an internal stress σ_{id} that allows a deviatoric stress τ_o to generate a hydrostatic strain $\varepsilon_{o(d)}$.

By using Kotsovos' model, the complete stress-strain profile for actively confined concrete subjected to any combination of constant lateral pressures can be obtained. The model assumes that the axial stress is the major principal stress σ_1, and the lateral confining stresses σ_2 and σ_3 are known (or can be assumed). The model then gives the variation of the corresponding strains as the axial load changes.

A key feature in Kotsovos' model is the point he identifies as OUFP: the Onset of Unstable Fracture Process. For an actively confined sample, this marks the peak on the stress-strain curve. Before this point is reached, the axial strain on the concrete increases with axial load; after this point, the strain continues to increase but at decreasing load. For the passively confined concrete considered in the following, this point still exists but it does not necessarily mark the peak load.

For completeness, the detailed equations are given in the Appendix. The procedures can be summarized as follows:

1. The values of σ_2 and σ_3 are fixed;
2. The value of σ_1 that corresponds to OUFP is then calculated;
3. The ascending portions of the axial stress-axial strain and axial stress-lateral strain curves are calculated; and
4. For the post-OUFP state, the variation of the stress state $\delta\sigma_i$ and strain state $\delta\varepsilon_i$ (i = 1, 2, 3) can then be found.

This formulation is applicable to concrete subjected to constant (active) confining pressure. When concrete is surrounded by reinforcement, however, it is subjected to a passive confining pressure; the established model is not adequate because the confining pressures are not known.

ANALYTICAL MODELING OF CONCRETE WITH SINGLE SPIRAL

When spiral reinforcement is used to provide lateral pressure to the concrete, the confining pressure varies throughout the course of loading. With a linear-elastic confining material, like aramid, the confining pressure continues to increase until the spiral breaks, but with an elasto-plastic material, like steel, the pressure plateaus when the steel yields. The linear elastic case will be considered first and then modified to allow for steel plasticity.

Consider a circular concrete cylinder reinforced with a single spiral whose properties are known. Symmetry requires that $\sigma_2 = \sigma_3 = \sigma_L$; final failure is expected when the spiral snaps, which is not usually at the peak load. The analysis can be performed in the following steps, which are shown diagrammatically in Fig. 2:

1. Compatibility between the transverse concrete strain ε_2 and the strain of the confining spiral reinforcement ε_{sp} is

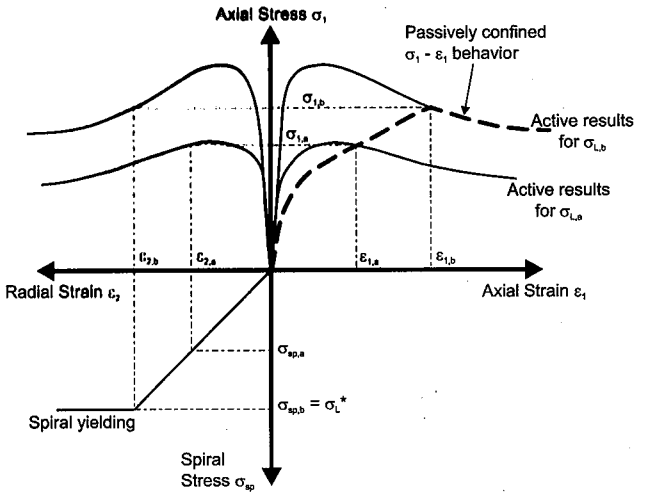

Fig. 3—Schematic model for passive steel confinement.

assumed, so $\varepsilon_2 = \varepsilon_{sp}$. The breaking strain of the spiral ε_{sp}^u then defines the ultimate lateral strain ε_2^u.

2. The relationship between the tensile stress in the spiral, σ_{sp}, and the spiral strain ε_{sp} is known

$$\sigma_{sp} = E_{sp}\varepsilon_{sp} = E_{sp}\varepsilon_2 \quad 0 \le \varepsilon_2 \le \varepsilon_2^u \tag{1}$$

where E_{sp} denotes the elastic modulus of spiral.

3. For any given ε_2, the equivalent active confining stress σ_L (= $\sigma_2 = \sigma_3$) is then calculated by

$$\sigma_L = \frac{2A_{sp}}{d_c s}\left(1 - \frac{s}{d_c}\right)E_{sp}\varepsilon_2 \tag{2}$$

where A_{sp} is the cross section area of spiral, d_c is the diameter of confined concrete, and s is the spiral spacing; the term $(1 - s/d_c)$ reduces the confining effect as the spiral pitch increases and implicitly assumes that $s < d_c$.

4. The σ_1-ε_2 and σ_1-ε_1 curves are generated for the calculated σ_L using Kotsovos' active model, as described previously. The axial stress σ_1 that generates the assumed value of ε_2 is then determined from the σ_1-ε_2 curve.

5. The corresponding value of ε_1 can then be found from the σ_1-ε_1 curve. This represents one point on the passive stress-strain response of the specimen.

6. By repeating Procedures (2) to (5) for a range of values of ε_{sp} from 0 to ε_{sp}^u, the complete σ_1-ε_1 profile for the passively confined concrete cylinder can then be established.

The procedure is slightly modified when steel reinforcement is used, as illustrated in Fig. 3. The confining stress reaches a limiting value (at σ_L^*) when the steel reaches its yield point, but it continues to sustain a load as the steel yields with the confining stress remaining effectively constant. The stress-strain curve of the steel-confined concrete then follows the active σ_1-ε_1 curve for σ_L^*.

It should be noted that OUFP does not play a particularly important role in the behavior of passively confined concrete. The confined concrete can be identified as being before or after OUFP, and the slope of the resulting stress-strain curve changes as this point is passed, but it does not necessarily indicate the peak load that the concrete can sustain. The confining pressure will continue to increase beyond OUFP, usually by a significant amount, and this may be sufficient to allow the concrete to carry further axial load. The ultimate failure, which will probably not occur at the peak load, occurs when the spiral snaps. At this point, the confining action suddenly disappears and the concrete can be expected to disintegrate.

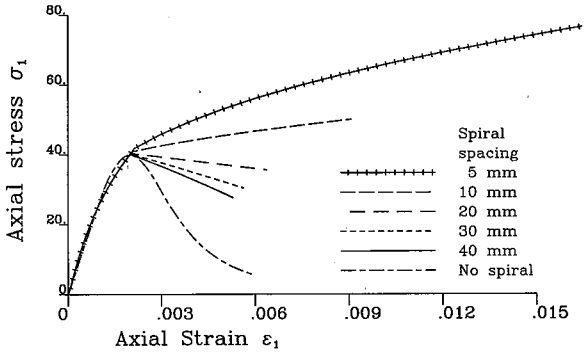

Fig. 4—Effect of varying spiral spacing (f_c = 40 MPa, aramid spirals).

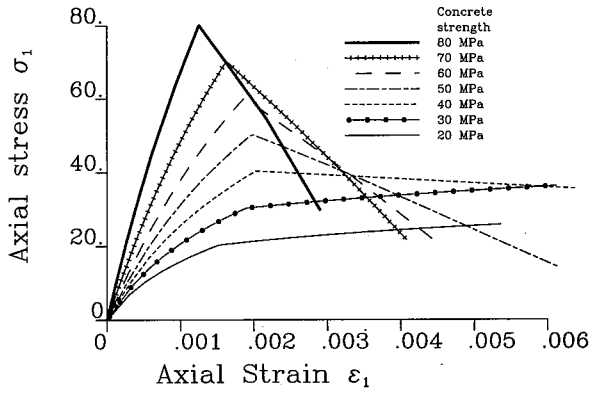

Fig. 5—Effect of varying concrete strength (aramid spirals, spacing = 20 mm).

Results for actively confined concrete

All the results presented in this section are for a circular cylinder confined within a spiral of aramid reinforcement.[2] The diameter of the spiral is 90 mm, with a cross-sectional area of 5.3 mm^2. The effective strength of the spiral is 456 MPa at a strain of 1.53%. The uniaxial cylinder strength of the concrete is varied, as is the spiral spacing.

The effect of varying the spiral pitch is shown in Fig. 4 for concrete with a strength of 40 MPa. Reducing the spiral pitch increases the strain capacity of the concrete; for s less than approximately 15 mm, the concrete gains strength and a significant enhancement of capacity is predicted for spacings of 5 mm. Also shown in Fig. 4 is the σ_1-ε_1 response for unconfined concrete, as predicted by Carreira and Chu.[20] It can be seen that the confining reinforcement has very little effect until internal fracture starts to occur in the concrete with a corresponding increase in specimen volume.

The effect of varying concrete strength is shown in Fig. 5. The spiral spacing is held constant at 20 mm, but the concrete strength is varied from 20 to 80 MPa. (It should be noted here that Kotsovos' equations are only calibrated up to 65 MPa). As expected, the stiffness increases as the concrete gets stronger, but the beneficial effects of the confinement are reduced; stiffer concrete produces less lateral expansion, so the confining stress is reduced in real terms, and even

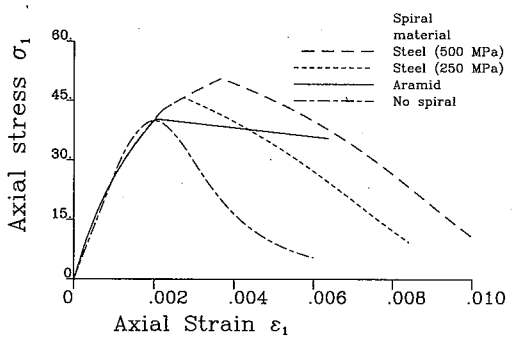

Fig. 6—Comparison between use of aramid and steel spirals of different strengths.

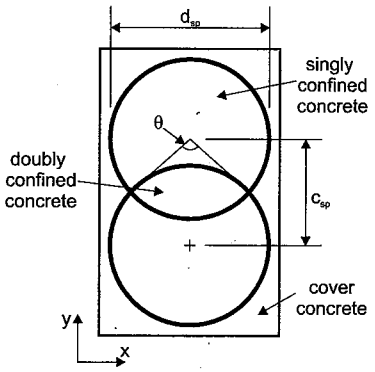

Fig. 7—Concrete section with two interlocking spirals.

more so as a proportion of the concrete strength. This shows that weaker concrete can benefit from the effects of confinement, but for stronger concrete the effects are much less marked. If the objective is to maximize the energy dissipation by increasing the area under the stress-strain curve, then the use of a moderate concrete strength (≈40 MPa) is preferable to the use of very high-strength concrete. The numerical results also showed that for high-strength concrete (>60 MPa), the spirals did not reach their ultimate strength, with the concrete strength reducing to negligible values before the spiral snapped.

The effect of using steel for confinement is shown in Fig. 6 for concrete with a strength of 40 MPa and a spiral pitch of 20 mm. Results are shown for steel with yield strengths of 250 and 500 MPa (Young's modulus 200 GPa and cross-sectional area 5.3 mm^2). The additional stiffness of the steel increases the passive strength of the concrete above that of the aramid spirals, but when the steel yields, no further enhancement of strength occurs and the applied stress drops rapidly.

CONCRETE WITH TWO INTERLOCKING SPIRALS

The analysis given previously applies to axisymmetric cylinders. For sections with overlapping spirals, the confining stresses σ_2 and σ_3 cannot be expressed as simple functions of the spiral strain and will also not be equal. Thus, the degree of confinement can be expected to vary and a method is required that allows the σ_1-ε_1 curve to be obtained for the more realistic situation.

One possibility is to perform a global analysis of a beam using a finite element analysis that incorporates Kotsovos' model and also includes the spirals themselves as discrete elements. In general applications, however, it will not be sensible to perform a finite element analysis each time; instead, a method is sought that allows the effects of the interlock to be taken into account more easily.

Consider the case of concrete reinforced with two interlocking spirals. The concrete inside the overlapping area experiences a higher confining stress than that in the outer areas because it is under stress induced by both spirals simultaneously. If the uniform confining stress induced by a single spiral is σ_L, then the concrete inside the interlocking area must be subjected to a stress between σ_L and $2\sigma_L$. The concrete in the outer area might also be affected by the interlocking action but the variation can be expected to be significantly smaller.

If two interlocking spirals are placed inside a rectangular column, the cross section can be divided into three zones: a doubly confined area, a singly confined area, and cover concrete (Fig. 7). Inside the doubly confined area of concrete, the spacing of the spiral can be idealized as being half that of the singly confined area, assuming the spirals have equal pitch. The lateral pressure on the inner boundary of the doubly confined area is larger than that on the outer boundary of the singly confined area. Tanaka and Park[1] used the concept of the volumetric ratio of spirals and pointed out that the degree of confinement for the compression zone in the extremities of the core section confined by interlocking spirals may be less than that in the rest of the interlocking area. This is due to the uneven lateral pressure distribution that is generated. To take this into consideration, global x-y axes are defined and the coordinate system is applied to the layout of interlocking spirals (Fig. 7). It is proposed that magnifying factors k should be used to allow for the variation in confining stress in the two areas. Separate factors will be used for singly confined and doubly confined regions, with different factors for the x- and y-directions, giving a total of four factors.

For the singly confined area,

$$\sigma_X^{sc} = \frac{2A_{sp}}{d_c s}\left(1 - \frac{s}{d_c}\right)\sigma_{sp}k_{LX}^{sc} = \sigma_L k_{LX}^{sc} \quad (3)$$

$$\sigma_Y^{sc} = \frac{2A_{sp}}{d_c s}\left(1 - \frac{s}{d_c}\right)\sigma_{sp}k_{LY}^{sc} = \sigma_L k_{LY}^{sc} \quad (4)$$

For the doubly confined area,

$$\sigma_X^{dc} = \frac{2A_{sp}}{d_c s}\left(1 - \frac{s}{d_c}\right)\sigma_{sp}k_{LX}^{dc} = \sigma_L k_{LX}^{dc} \quad (5)$$

$$\sigma_Y^{dc} = \frac{2A_{sp}}{d_c s}\left(1 - \frac{s}{d_c}\right)\sigma_{sp}k_{LY}^{dc} = \sigma_L k_{LY}^{dc} \quad (6)$$

The values of k_{LX} and k_{LY} largely depend on the ratio of the center-to-center distance c_{sp} of the two interlocking spirals to the diameter of spiral d_{sp}. Using the same pitch for the two spirals, the variations of the correction factor in two orthogonal directions in both the doubly and singly confined areas can be determined by means of a finite element analysis.

The finite element analysis assumes that the concrete is linearly elastic and that each spiral induces a uniform inward pressure, which is equivalent to stating that stress in the

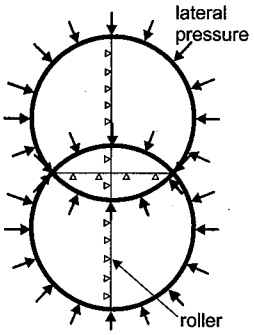

Fig. 8—Layout of finite element model.

spirals is constant around the complete loop. The principal stresses induced at each node in the two confined zones are determined, but because the orientation of the principal directions vary over the section, the stresses in two fixed orthogonal directions are calculated. These are then averaged over the two regions to give the four values for the correction factor. These correction factors are then used to vary the lateral stresses applied in the actively confined analysis.

A notional lateral pressure of 100 units was assumed. The nodes along the axes of symmetry, and those along the spirals themselves, were specified and an automatic mesh generator then produced the rest of the nodes inside the spirals. Triangular elements were adopted throughout; typically about 1000 elements were used.

The nodes along the axes of symmetry were restrained by roller support conditions to maintain symmetry (Fig. 8). A plane-strain linear-elastic material was assumed because the object of the exercise was to determine the magnitudes of the principal stresses everywhere.

In forming the best-fit equation, c_{sp}/d_{sp} is used as the parameter indicating the degree of overlapping of the spirals. A third-order least-squares fitting is used, and the magnification factors for the singly and doubly confined portions of concrete in the two global directions are determined separately.

For the singly confined areas,

$$k_{LX}^{sc} = 1.3721 - 1.2103\left(\frac{c_{sp}}{d_{sp}}\right) + 1.5177\left(\frac{c_{sp}}{d_{sp}}\right)^2 - 0.6835\left(\frac{c_{sp}}{d_{sp}}\right)^3 \quad (7)$$

$$k_{LY}^{sc} = 1.3059 - 0.8711\left(\frac{c_{sp}}{d_{sp}}\right) + 0.8657\left(\frac{c_{sp}}{d_{sp}}\right)^2 - 0.3017\left(\frac{c_{sp}}{d_{sp}}\right)^3 \quad (8)$$

whereas for the doubly-confined areas,

$$k_{LX}^{dc} = 1.9999 - 0.8869\left(\frac{c_{sp}}{d_{sp}}\right) + 1.5434\left(\frac{c_{sp}}{d_{sp}}\right)^2 - 1.3374\left(\frac{c_{sp}}{d_{sp}}\right)^3 \quad (9)$$

$$k_{LY}^{dc} = 1.9913 - 0.4046\left(\frac{c_{sp}}{d_{sp}}\right) + 0.2178\left(\frac{c_{sp}}{d_{sp}}\right)^2 + 0.1615\left(\frac{c_{sp}}{d_{sp}}\right)^3 \quad (10)$$

These expressions are plotted in Fig. 9 for $0 < c_{sp}/d_{sp} < 1$. When $c_{sp}/d_{sp} = 0$, a complete overlap is formed and there is no singly confined area; k_x^{dc} and k_y^{dc} are both 2, as would be expected. When $c_{sp}/d_{sp} = 1$, the two spirals touch each other and there is no doubly confined region; k_x^{sc} and k_y^{sc} are both 1, again as would be expected.

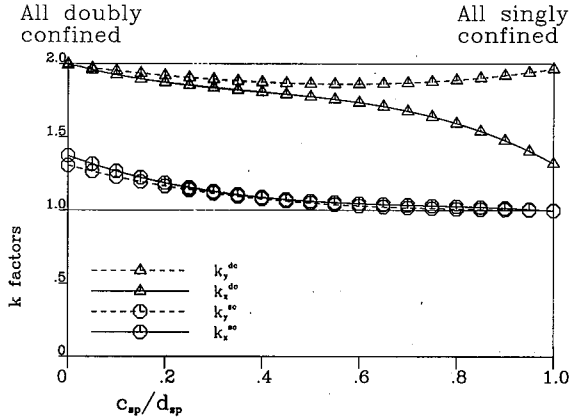

Fig. 9—Variation of magnification factors with degree of overlap of spirals.

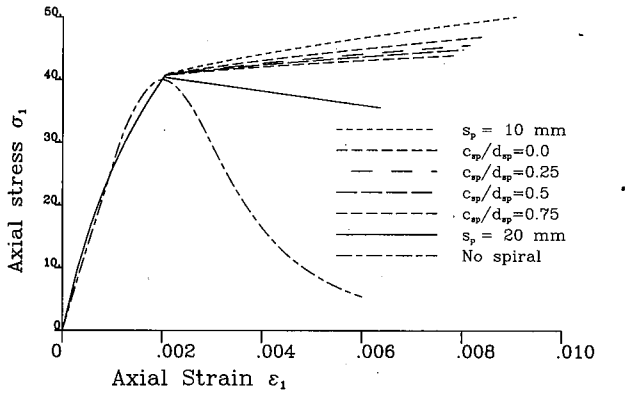

Fig. 10—Effect of degree of overlap on behavior of doubly confined concrete.

The analysis then proceeds as before, with Eq. (3) to (6) replacing Eq. (2), using the appropriate k factors obtained from Eq. (7) to (10). These specify revised values for the lateral stresses σ_2 and σ_3, which are then used in the active analysis.

It must be stressed that, in the analysis given herein, it is assumed that the strain in the spiral takes a constant average value, which is given by $\varepsilon_{sp} = \varepsilon_2$. This allows the assumption that the inward pressure from the spiral is uniform, and hence allows the use of the k factors determined from the finite element analysis. If this assumption is not made, it would be necessary to perform detailed finite element analyses to see how the spiral strain varied around the circle.

Figure 10 shows the passive confinement responses for a concrete with a strength of 40 MPa and aramid spirals with a pitch of 20 mm. The responses for the doubly confined concrete with four different c_{sp}/d_{sp} values are shown. There is a small variation with this factor, but it is not significant. Also shown are the responses for singly reinforced concrete with spacings of 20 and 10 mm. The response for $s_p = 10$ mm is not the same as that for $c_{sp}/d_{sp} = 0.0$ because of the effect of the $(1 - s/d_c)$ term; doubling the area of the spiral does not produce exactly the same effect as halving the spacing due to the reduced confinement between the spirals.

When determining the overall load-extension response of an element containing all three types of concrete, the stress-strain curves for each element should be multiplied by the appropriate cross-sectional area. Due to the differences in the stress state of the singly confined area and doubly

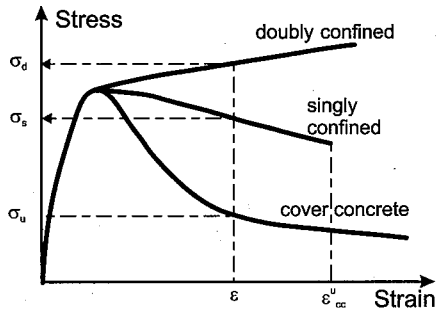

Fig. 11—Stress-strain curves for three different types of concrete.

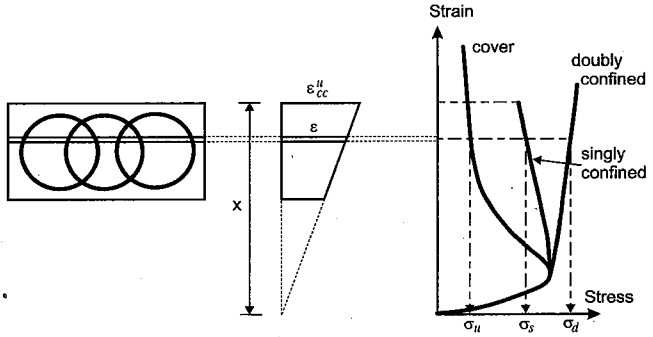

Fig. 12—Eccentric analysis of concrete with interlocking spirals.

confined areas, the end-points of these stress-strain curves are different. It is postulated that the section reaches its failure state when the first spiral snapping occurs, at which point the confinement ceases to be effective and the concrete becomes unconfined. Therefore, the smaller strain value of the two end-points gives the failure strain of the concrete with interlocked spirals ε_{cc}^{u} (Fig. 11).

ECCENTRIC ANALYSIS FOR CONCRETE WITH INTERLOCKING SPIRALS

The analysis thus far has assumed that the external force is applied axially so that the resulting force is aligned with the center of the specimen and the axial strain is uniform across the section. If this analysis is to be applied to the compression zones of beams, however, the strain can be expected to vary across the section.

If it is assumed that the stress-strain curves for unconfined, singly confined, and doubly confined concrete, as determined previously, are still valid, then it is possible to use these to determine the force/moment versus axial strain/curvature relationships as required.

For example, to determine the ultimate value of the axial force applied at a fixed eccentricity e, the position of the neutral axis of the section can be varied until the resulting force and moment match the required eccentricity. Failure is assumed to occur when the confined concrete reaches its ultimate strain ε_{cc}^{u}. It is assumed that when concrete is subjected to a tensile strain, it cracks and carries no load. The procedure can be summarized as follows:

1. Determine the eccentricity e from the applied force and moment;
2. Assume a neutral axis depth x;
3. The concrete section is then divided into small slices; each may contain three kinds of elements. By assuming that the ultimate strain of the confined concrete, ε_{cc}^{u}, is reached at the most confined edge, the strain at the middle of each element can be calculated;
4. The appropriate stress-strain model for both confined and unconfined areas is then used, from which the corresponding stress values are determined (Fig. 12);
5. The axial force N, moment M, and corresponding eccentricity are obtained by summing the effects of the elemental stress and the associated area;
6. If e does not equal the chosen eccentricity, the neutral axis depth is adjusted and the process repeated until a satisfactory value is obtained; and
7. The curvature κ and axial strain ε_a are then calculated.

It should be noted that this analysis requires that the strain in the spiral varies across the depth of the compression zone and takes the value it would have had if a uniaxial compressive strain of the appropriate value were applied to the section. This is not necessarily the case but is a reasonable assumption.

This procedure can be adapted easily to find other relationships; for example, to determine the moment-curvature relationship for a given value of e, the extreme fiber strain can be varied from zero up to the failure value assumed previously.

CONCLUSIONS

It has been shown that Kotsovos' model for triaxially confined concrete can be used to determine the behavior of concrete contained within passive spirals of reinforcement. This has been applied to cylinders reinforced with spirals of aramid fibers and the effects of varying both the spiral pitch and the concrete strength have been studied. High-strength concrete does not benefit significantly from confinement because it is stiffer and does not generate sufficient lateral expansion to mobilize the confining stress. The best effect of confinement (in terms of the energy dissipated) is obtained for concretes of moderate strength.

The differences associated with the use of steel reinforcement have been studied. Steel is more effective at providing confinement up to yield, due to the higher stiffness, but once the steel yields, the strength drops off rapidly.

It has been shown that the area contained within the overlapping region of two spirals can be studied by the use of a finite element analysis. This allows the effect of the varying geometry on the confining stresses to be determined, which can then be used in the passive model to obtain different stress-strain curves for the singly and doubly confined regions.

Finally, it has been shown how the model can be used to determine the behavior of confined concrete in the compression zone of beams where the strain varies through the depth.

ACKNOWLEDGMENTS

The first author was supported in this work by the Croucher Foundation whose support is gratefully acknowledged.

NOTATION

A_{sp}	=	cross-sectional area of spiral
d_c	=	diameter of spiral
E_{sp}	=	Young's modulus of spiral
e	=	eccentricity of compressive force
k_{LX}^{sc} and k_{LY}^{sc}	=	magnification factors in x- and y-directions for singly confined concrete
k_{LX}^{dc} and k_{LY}^{dc}	=	magnification factors in x- and y-directions for doubly confined concrete
M	=	moment on compression zone
N	=	compression force
s	=	pitch (spacing) of spiral
x	=	neutral axis depth

$\delta\varepsilon_i$ = variation in principal strain (i = 1, 2, 3)
$\delta\sigma_i$ = variation in principal stress (i = 1, 2, 3)
ε_1 = axial strain in concrete cylinder
ε_2 = lateral strain on concrete cylinder
ε_a = axial strain on concrete beam
ε_2^u = maximum lateral strain in concrete
ε_{sp} = strain in spiral
ε_{sp}^u = breaking strain of spiral
$\varepsilon_{o(d)}$ = hydrostatic strain caused by internal stress
κ = curvature
σ_1, σ_2, and σ_3 = principal stresses
σ_{id} = internal stress
σ_L = lateral confining stress
σ_L^* = limiting confining stress when steel spirals used
σ_o = hydrostatic stress
σ_{sp} = stress in spiral
τ_o = deviatoric stress

REFERENCES

1. Tanaka, H., and Park, R., "Seismic Design and Behavior of Reinforced Concrete Columns with Interlocking Spirals," *ACI Structural Journal*, V. 90, No. 2, Mar.-Apr. 1993, pp. 192-203.
2. Leung, H. Y., "Aramid Fibre Spirals to Confine Concrete in Compression," PhD thesis, University of Cambridge, UK, 2000, 200 pp.
3. Choi, S.; Thienel, K. C.; and Shah, S. P., "Strain Softening of Concrete in Compression under Different End Constraints," *Magazine of Concrete Research*, V. 48, No. 175, 1996, pp. 103-115.
4. Hsu, L. S., and Hsu, C. T. T., "Complete Stress-Strain Behaviour of High-Strength Concrete under Compression," *Magazine of Concrete Research*, V. 46, No. 169, 1994, pp. 301-312.
5. Imran, I., and Pantazopoulou, S. J., "Experimental Study of Plain Concrete under Triaxial Stress," *ACI Materials Journal*, V. 93, No. 6, Nov.-Dec. 1996, pp. 589-601.
6. Kotsovos, M. D., and Pavlovic, M. N., *Structural Concrete*, Thomas Telford, London, 1995, 550 pp.
7. Lahlou K.; Aitcin, P. C.; and Chaallal, O., "Behaviour of High-Strength Concrete under Confined Stresses," *Cement & Concrete Composites*, V. 14, 1992, pp. 185-193.
8. Mansur, M. A.; Wee, T. H.; and Chin, M. S., "Derivation of the Complete Stress-Strain Curves for Concrete in Compression," *Magazine of Concrete Research*, V. 47, No. 173, 1995, pp. 285-290.
9. Morales, S. M.; Nilson, A. H.; and Slate, F. O., "Spirally-Reinforced High-Strength Concrete Columns," *Report* No. 82-10, Cornell University, Ithaca, N.Y., 1982, 255 pp.
10. Kotsovos, M. D., and Newman, J. B., "Behavior of Concrete under Multiaxial Stress," ACI JOURNAL, *Proceedings* V. 74, No. 9, Sept. 1977, pp. 443-446.
11. Kotsovos M. D., "Consideration of Triaxial Stress Conditions in Design: A Necessity," *ACI Structural Journal*, V. 84, No. 3, May-June 1987, pp. 266-273.
12. Kotsovos, M. D., and Pavlovic, M. N., *Ultimate Limit-State Design of Concrete Structures: A New Approach*, Thomas Telford, London, 1999, 208 pp.
13. Mander, J. B.; Priestley, M. J. N.; and Park, R., "Theoretical Stress-Strain Behavior of Confined Concrete," *Journal of Structural Engineering*, ASCE, V. 114, No. 8, 1988, pp. 1804-1826.
14. Mander, J. B.; Priestley, M. J. N.; and Park, R., "Observed Stress-Strain Behavior of Confined Concrete," *Journal of Structural Engineering*, ASCE, V. 114, No. 8, 1988, pp. 1827-1849.
15. Mander, J. B.; Priestley, M. J. N.; and Park, R., closure of "Observed Stress-Strain Behavior of Confined Concrete," *Journal of Structural Engineering*, ASCE, V. 117, No. 2, 1991, pp. 628-629.
16. Richart, F. E.; Brandtzaeg, A.; and Brown, R. L., "A Study of the Failure of Concrete under Combined Compressive Stresses," *University of Illinois Engineering Experiment Station Bulletin* No. 185, 1928.
17. Saadatmanesh, H.; Ehsani, M. R.; and Li, M. W., "Strength and Ductility of Concrete Columns Externally Reinforced with Fiber Composite Straps," *ACI Structural Journal*, V. 91, No. 4, July-Aug. 1994, pp. 434-447.
18. Kotsovos, M. D., and Newman, J. B., "A Mathematical Description of the Deformational Behaviour of Concrete under Complex Loading," *Magazine of Concrete Research*, V. 31, No. 107, 1979, pp. 77-90.
19. Kotsovos, M. D., and Newman, J. B., "Mathematical Description of Deformational Behavior of Concrete under Generalized Stress beyond Ultimate Strength," ACI JOURNAL, *Proceedings* V. 77, No. 5, Sept.-Oct. 1980, pp. 340-346.
20. Carreira, D. J., and Chu, K.-H., "Stress-Strain Relationship for Plain Concrete in Compression," ACI JOURNAL, *Proceedings* V. 82, No. 6, Nov.-Dec. 1985, pp. 797-804.

APPENDIX—KOTSOVOS' MODEL FOR ACTIVE CONFINEMENT

This appendix simply lists the equations used in the active analysis. Full details and explanations are to be found in Kotsovos' papers.[6,19] The numerical values have been obtained by curve-fitting to experimental results obtained from triaxial tests. All equations assume that stresses and elastic moduli are expressed in MPa.

The model works in terms of hydrostatic stress σ_o and deviatoric stress τ_o invariants defined by

$$\sigma_o = \frac{\sigma_1 + \sigma_2 + \sigma_3}{3} = \frac{z}{\sqrt{3}} \tag{A1}$$

$$\tau_o = \frac{1}{3}\sqrt{(\sigma_1 - \sigma_2)^2 + (\sigma_2 - \sigma_3)^2 + (\sigma_3 - \sigma_1)^2} = \frac{r}{\sqrt{3}} \tag{A2}$$

and

$$\cos\vartheta = \frac{1}{r\sqrt{6}}(\sigma_1 + \sigma_2 - 2\sigma_3) \tag{A3}$$

The uniaxial strength of the concrete is σ_c^u.

Onset of unstable fracture process

The peak of the stress-strain curve occurs at a point that Kotsovos identified as OUFP—the Onset of Unstable Fracture Process. This occurs when the applied stress-invariants σ_o^u and τ_o^u satisfy

$$\tau_o^u = \frac{2\tau_{oc}(\tau_{oc}^2 - \tau_{oe}^2)\cos\vartheta}{4(\tau_{oc}^2 - \tau_{oe}^2)\cos^2\vartheta + (\tau_{oc} + 2\tau_{oe})^2} + \frac{\tau_{oc}(2\tau_{oe} - \tau_{oc})\sqrt{4(\tau_{oc}^2 - \tau_{oe}^2)\cos^2\vartheta + 5\tau_{oe}^2 - 4\tau_{oc}\tau_{oe}}}{4(\tau_{oc}^2 - \tau_{oe}^2)\cos^2\vartheta + (\tau_{oc} + 2\tau_{oe})^2} \tag{A4}$$

where

$$\frac{\tau_{oc}}{\sigma_c^u} = 0.944\left(\frac{\sigma_o^u}{\sigma_c^u} + 0.05\right)^{0.724} \tag{A5}$$

and

$$\frac{\tau_{oe}}{\sigma_c^u} = 0.633\left(\frac{\sigma_o^u}{\sigma_c^u} + 0.05\right)^{0.857}$$

Ascending curve

The initial values of the bulk and shear moduli are given by

$$K_e = 11{,}000 + 3.2(\sigma_c^u)^2 \tag{A6}$$

and

$$G_e = 9224 + 136\sigma_c^u + 3296 \times 10^{-15}(\sigma_c^u)^{8.273}$$

When $\sigma_c^u \le 31.7$ MPa

$$\begin{aligned} A_k &= 0.516 \\ C_k &= 3.573 \\ d_k &= 2.12 + 0.0183 \times \sigma_c^u \\ m_k &= -2.415 \\ n_k &= 1.0 \end{aligned} \tag{A7}$$

When $\sigma_c^u > 31.7$ MPa

$$\begin{aligned} A_k &= \frac{0.516}{1 + 0.0027(\sigma_c^u - 31.7)^{2.397}} \\ C_k &= \frac{3.573}{1 + 0.0134(\sigma_c^u - 31.7)^{1.414}} \\ d_k &= 2.7 \\ m_k &= -3.531 + 0.0352\sigma_c^u \\ n_k &= 0.3124 + 0.0217\sigma_c^u \end{aligned} \tag{A8}$$

In all cases

$$\begin{aligned} b_k &= 2.0 + 1.81 \times 10^{-8}(\sigma_c^u)^{4.461} \\ k_k &= \frac{4.0}{1 + 1.087(\sigma_c^u - 15.0)^{0.23}} \\ l_k &= 0.222 + 0.01086\sigma_c^u - 0.000122(\sigma_c^u)^2 \end{aligned} \tag{A9}$$

When $\sigma_o/\sigma_c^u \le 2$

$$\frac{K_s}{K_e} = \frac{1}{1 + A_k\left(\frac{\sigma_o}{\sigma_c^u}\right)^{b_k - 1}} \tag{A10}$$

When $\sigma_o/\sigma_c^u > 2$

$$\frac{K_s}{K_e} = \frac{1}{1 + 2^{b_k - 1}A_k b_k - 2^{b_k}(b_k - 1)A_k\left(\frac{\sigma_o}{\sigma_c^u}\right)^{b_k - 1}} \tag{A11}$$

In all cases

$$\begin{aligned} \frac{G_s}{G_e} &= \frac{1}{1 + C_k\left(\frac{\tau_o}{\sigma_c^u}\right)^{d_k - 1}} \\ E_s &= \frac{9K_sG_s}{3K_s + G_s} \\ v_s &= \frac{3K_s - 2G_s}{6K_s + 2G_s} \end{aligned} \tag{A12}$$

then

$$M_k = \frac{k_k}{1 + l_k\left(\frac{\sigma_o}{\sigma_c^u}\right)^{m_k}} \tag{A13}$$

$$\begin{aligned} \frac{\sigma_{id}}{\sigma_c^u} &= M_k\left(\frac{\tau_o}{\sigma_c^u}\right)^{n_k} \\ \varepsilon_1 &= \left(\frac{\sigma_1 + \sigma_{id}}{2G_s}\right) - \frac{3v_s}{E_s}(\sigma_o + \sigma_{id}) \\ \varepsilon_2 &= \left(\frac{\sigma_2 + \sigma_{id}}{2G_s}\right) - \frac{3v_s}{E_s}(\sigma_o + \sigma_{id}) \end{aligned} \tag{A14}$$

This allows the construction of the ascending σ_1-ε_1 and σ_1-ε_2 curves up to OUFP.

Descending curve after OUFP

For $\sigma_c^u \le 31.7$

$$\begin{aligned} P_1 &= 3.6167 \\ S &= 1.07 \\ T &= 0.276 \end{aligned} \tag{A15}$$

For $\sigma_c^u > 31.7$

$$\begin{aligned} P_1 &= \frac{3.6167}{1 + 0.0382(\sigma_c^u - 31.7)^{1.945}} \\ S &= \frac{1.07}{1 + 0.0186(\sigma_c^u - 31.7)^{1.589}} \\ T &= \frac{0.276}{1 + 0.0230(\sigma_c^u - 31.7)^{1.496}} \end{aligned} \tag{A16}$$

In all cases

$$\begin{aligned} Q_1 &= 0.0546 - 0.0174\sigma_c^u + 0.0003(\sigma_c^u)^2 \\ R_1 &= 6.3822 - 0.1953\sigma_c^u + 0.0018(\sigma_c^u)^2 \\ P_2 &= -19.992 + 0.4804\sigma_c^u - 0.0032(\sigma_c^u)^2 \\ Q_2 &= 20.897 - 0.5806\sigma_c^u + 0.0043(\sigma_c^u)^2 \\ R_2 &= 6.1928 - 0.1363\sigma_c^u + 0.001(\sigma_c^u)^2 \end{aligned} \tag{A17}$$

$$F_1 = \frac{P_1}{1 + Q_1\left(\frac{\sigma_o}{\sigma_c^u}\right)^{R_1}} \tag{A18}$$

For $\sigma_o/\sigma_c^u \le 0.8$

$$F_2 = \frac{P_2}{1 + Q_2\left(\frac{\sigma_o}{\sigma_c^u}\right)^{R_2}} \quad \text{(A19)}$$

For $\sigma_o/\sigma_c^u > 0.8$

$$F_2 = \frac{P_2}{1 + Q_2 \times 0.8^{R_2}} + \frac{0.25\left(\frac{\sigma_o}{\sigma_c^u}\right) - 0.2}{\left(\frac{\sigma_o}{\sigma_c^u}\right) + 0.2} \quad \text{(A20)}$$

For $\sigma_o/\sigma_c^u \leq 2S/3T$

$$X_1 = \left[S - T \times \left(\frac{\sigma_o}{\sigma_c^u}\right)\right]\left(\frac{\sigma_o}{\sigma_c^u}\right)^2 \quad \text{(A21)}$$

For $\sigma_o/\sigma_c^u > 2S/3T$

$$X_1 = \frac{4S^3}{27T^2} \quad \text{(A22)}$$

In all cases

$$f_1 = \left(\frac{\vartheta}{60}\right)^{0.2}$$
$$f_2 = \frac{1}{F_2} + \left(1 - \frac{1}{F_2}\right)\left(\frac{\vartheta}{60}\right) \quad \text{(A23)}$$
$$f_3 = 2f_1 - f_2$$

$$\delta\varepsilon_o = (F_1 + X_1)\delta\tau_o f_1 \quad \text{(A24)}$$

$$r_{21} = F_2 f_2$$
$$r_{31} = F_2 f_3 \quad \text{(A25)}$$

$$\delta\varepsilon_1 = \frac{3\delta\varepsilon_o}{1 + r_{21} + r_{31}}$$
$$\delta\varepsilon_2 = r_{21}\delta\varepsilon_1 \quad \text{(A26)}$$
$$\delta\varepsilon_3 = r_{31}\delta\varepsilon_1$$

These additional strains are added to the strain state at OUFP. Note that these strains are in mm/m and therefore have to be divided by 1000 to give true strain.